Thermal diffusion by Brownian-motion-induced fluid stress

Jennifer Kreft[1] and Yeng-Long Chen[1,2,*]
[1]*Institute of Physics, Academia Sinica, Taipei, Taiwan*
[2]*Research Center for Applied Science, Academia Sinica, Taipei, Taiwan*
(Received 8 February 2007; published 10 August 2007)

The Ludwig-Soret effect, the migration of a species due to a temperature gradient, has been extensively studied without a complete picture of its cause emerging. Here we investigate the dynamics of DNA and spherical particles subjected to a thermal gradient using a combination of Brownian dynamics and the lattice Boltzmann method. We observe that the DNA molecules will migrate to colder regions of the channel, an observation also made in experiments. In fact, the thermal diffusion coefficient found agrees quantitatively with the experimentally measured value. We also observe that the thermal diffusion coefficient decreases as the radius of the studied spherical particles increases. Furthermore, we observe that the thermal-fluctuation–fluid-momentum-flux coupling induces a gradient in the stress which leads to thermal migration in both systems.

DOI: 10.1103/PhysRevE.76.021912 PACS number(s): 87.14.Gg, 66.30.Xj, 87.15.Vv

I. INTRODUCTION

The first observations of the migration of a species due to a temperature gradient were reported by Ludwig and Soret more than 100 years ago [1,2]. Since that time, the effect has been observed in many multicomponent systems including fluid mixtures, colloidal suspensions, and polymer solutions [3]. The mass flux of a species is described by Fick's law with an added term to account for thermal diffusion:

$$J_y = -\rho D\frac{dc}{dy} - \rho D_T c(1-c)\frac{dT}{dy}, \tag{1}$$

where J_y is the particle flux in the y direction. The first term denotes diffusion due to a density gradient: D is the molecular diffusion coefficient, c is the mass fraction of the migrating species, and ρ is the mass density. The second term describes diffusion due to the temperature gradient: D_T is the thermal diffusion coefficient and T is the temperature. At steady state, $J_y=0$ and the Soret coefficient, S_T is defined as

$$S_T \equiv \frac{D_T}{D} = -\frac{1}{c(1-c)}\frac{\partial c/\partial y}{\partial T/\partial y}. \tag{2}$$

Note that S_T can be positive or negative depending on whether the species migrates to the hot ($S_T<0$) or cold ($S_T>0$) region.

In general, the thermal diffusion coefficient for a molecule will depend on many factors [3]. For example, a recent simulation conducted on DNA tightly confined to nanometer-scale channels showed migration towards the heated region [4]. In contrast, experiments on DNA unconfined in the direction of the temperature gradient show the polymer migrating to the cold region [5]. Other factors shown in experiments to be important include the average temperature of the system, the solvent used, and electrostatic effects [6–8]. Interestingly, the polymer thermodiffusivity has been found to have weak or no dependence on the polymer molecular weight, unlike the polymer diffusivity [5,9,10]. However, the thermal diffusion coefficient has been shown to depend on the DNA length for certain values of the Debye length and salt concentration in [11], in contrast to the experiments in [5] which used a higher salt concentration.

Since many factors can play an important role in determining the thermal diffusion coefficient, theoretical predictions and experimental data sometimes do not agree. The experiments in [12] used colloidal particles of many different materials and showed that D_T will increase with increasing particle diameter a when some aqueous solutions are used to suspend the colloids and decrease with increasing a for others. These experiments suggest that the surface interactions between the particle and the solvent play important roles in the particles' thermodiffusion coefficient. Another experiment using carboxyl-modified polystyrene particles showed that D_T increases with increasing a. The authors propose a model based on local equilibrium conditions that predicts D_T will only increase with increasing a [13]. They observe this trend when the magnitude of the temperature gradient is much smaller than that in the experiments reported in [12]. They therefore surmise that the differences between their results and those in [12] are due to differences in the gradient magnitude and nonlinear effects in large gradients. Another model based on volume transport theory has proposed that D_T for dilute solutions of large molecules depends only on the solvent isobaric thermal expansion coefficient assuming that the pressure is uniform throughout the fluid [14,15].

Several theoretical studies have proposed that the thermal diffusion of colloids or polymers is a surface-driven phenomenon. This approach was first adopted by Ruckenstein [16]. Piazza and Guarino use this model to qualitatively predict the role of electrostatics in the thermal diffusion of charged micelles [8]. In general, these studies use hydrodynamic equations to calculate a pressure gradient and/or volume force acting locally on the particles that is induced by a nonuniform distribution of solvent molecules or temperature-dependent solvent-particle interaction [8,16–20]. Others also include a macroscopic pressure gradient due to the response of the solvent alone to the temperature gradient and this model nearly quantitatively reproduces the mobility of polymers as measured in experiments [17,21]. Another approach begins with the kinetic theory of diffusion in a nonuniform

*Corresponding author. yenglong@phys.sinica.edu.tw

temperature field to derive expressions for the Soret coefficient which allow for both positive and negative values of S_T [22].

Here, we present results from a lattice Boltzmann simulation of λ-DNA in a microchannel subjected to a thermal gradient that quantitatively agrees with published experimental values for the thermal diffusion coefficient. We show that a *nonequilibrium* stress develops from particle fluctuations. This component of the solvent characteristics causes thermal migration of the species. We also investigate the thermal diffusion of small, spherical particles and show that D_T decreases with increasing diameter, independent of the magnitude of the thermal gradient.

II. LATTICE BOLTZMANN WITH BROWNIAN DYNAMICS SIMULATION

We use a simulation based on the lattice Boltzmann method (LBM) for the fluid coupled with a wormlike chain (WLC) model with Brownian dynamics (BD) for the polymer [23–26]. The fundamental quantity in the LBM is the fluid velocity distribution function $n_i(\mathbf{r},t)$, which describes the fraction of fluid particles with a discretized velocity $\mathbf{c}_i$ at each lattice site [27,28]. To describe the velocities at each node, a 19 discrete velocity scheme in three dimensions is used. The velocities can be represented by $(0,0,0)$, $(\pm1,0,0)$, $(0,\pm1,0)$, $(0,0,\pm1)$, $(\pm1,\pm1,0)$, $(0,\pm1,\pm1)$, and $(\pm1,0,\pm1)$ and have magnitudes $c_i=|\mathbf{c}_i|=0$, 1, or $\sqrt{2}$. The maximum velocity in the simulation is given by the speed of sound: $c_s=\sqrt{1/3}\Delta x/\Delta\tau$ where Δx is the lattice spacing and $\Delta\tau$ is the time step. The distributions will be Maxwell-Boltzmann at equilibrium and can be represented by a second-order expansion

$$n_i^{eq}=\rho a^{ci}[1+(\mathbf{c}_i\cdot\mathbf{u})/c_s^2+\mathbf{uu}:(\mathbf{c}_i\mathbf{c}_i-c_s^2\mathbf{I})/(2c_s^4)], \quad (3)$$

where $\mathbf{u}$ is the local velocity. The coefficients a^{ci} are found by satisfying the isotropy condition

$$\sum_i a^{ci}\mathbf{c}_{i\alpha}\mathbf{c}_{i\beta}\mathbf{c}_{i\gamma}\mathbf{c}_{i\delta}=c_s^4(\delta_{\alpha\beta}\delta_{\gamma\delta}+\delta_{\alpha\gamma}\delta_{\beta\delta}+\delta_{\alpha\delta}\delta_{\beta\gamma}), \quad (4)$$

where α, β, γ, and δ represent the x, y, or z axis. The equilibrium conditions for the density ρ, momentum density $\mathbf{j}$, and momentum flux density $\mathbf{\Pi}$,

$$\rho=\sum_i n_i^{eq}, \quad (5)$$

$$\mathbf{j}=\rho\mathbf{u}=\sum_i \mathbf{c_i}n_i^{eq}, \quad (6)$$

$$\mathbf{\Pi}=\rho(\mathbf{uu}+c_s^2\mathbf{I})=\sum_i n_i^{eq}\mathbf{c_i}\mathbf{c_i}, \quad (7)$$

must also be satisfied.

At each time step, the fluid particles will collide with their nearest and next-nearest neighbors. The velocity distributions will evolve according to

$$n_i(\mathbf{r}+\mathbf{c}_i\Delta\tau,t+\Delta\tau)=n_i(\mathbf{r},t)+\mathbf{L}_{ij}[n_j(\mathbf{r},t)-n_j^{eq}(\mathbf{r},t)], \quad (8)$$

where $\mathbf{L}$ is a collision operator for fluid particle collisions such that the fluid always relaxes towards the equilibrium distribution. In the limit of small Knudson and Mach numbers, this equation has been shown to be equivalent to the Navier Stokes equation [29].

Collisions are simplified by transforming the n_i from velocity space into the hydrodynamic moments, $M_q=\mathbf{m}\cdot\mathbf{n}$, where M_q is the qth moment of the distribution, $\mathbf{m}$ is the transformation matrix, and $\mathbf{n}=(n_0,n_1,\ldots,n_{18})$. The density, momentum density, momentum flux, and the kinetic energy flux constitute the 19 moments; however, kinetic energy flux moments conserve energy and are considered "ghost" moments.

The collision operator is chosen to be a diagonal matrix with elements $\tau_0^{-1},\tau_1^{-1},\ldots,\tau_{18}^{-1}$ where τ_q is the characteristic relaxation time of the moment q. The conserved moments, density and momentum, are considered to have an infinite relaxation time and thus $\tau_{0,1,2,3}^{-1}=0$. The other moments have a single relaxation time τ_s, as in the Bhatanagar-Gross-Krook (BGK) model [30]. The relaxation time is constrained to be smaller than the fluid momentum diffusion time across the system, $\tau_s<\rho H^2/\eta$, where the shear viscosity η is given by $\eta=\rho c_s^2(\tau_s-0.5)$ for $\tau_s>0.5$ [29]. In our simulations, we have $\tau_s=1.0$.

A wormlike chain model is adopted for the λ-DNA in the simulation. The model has been parametrized to capture molecular dynamics in bulk solution at $T=298$ K and has been used to accurately predict the diffusivity of 48.5 kbps YOYO-stained DNA in microchannels [31–33].

Each molecule is represented by 11 beads connected by 10 wormlike springs. The position and velocity of the beads are updated using the explicit Euler method:

$$\mathbf{u}(t+\Delta t)=\mathbf{u}(t)+\mathbf{f}(t)\Delta t/m, \quad (9)$$

$$\mathbf{x}(t+\Delta t)=\mathbf{x}(t)+\mathbf{u}(t)\Delta t, \quad (10)$$

where $\mathbf{f}(t)$ is the total force acting on the bead, $\mathbf{u}(t)$ is the velocity, and $\mathbf{x}(t)$ is the position of the bead with mass m at time t. The time step for the beads is Δt. The forces acting on the bead include excluded-volume effects, the elastic force of the springs, hydrodynamic interactions with the solvent, and the Brownian motion of the particles.

The excluded-volume interactions between segments are calculated using a Gaussian excluded-volume potential that leads to self-avoiding walk statistics:

$$U_{ij}^{ev}=\frac{1}{2}k_BT\nu N_{ks}^2\left(\frac{3}{4\pi S_s^2}\right)\exp\left(\frac{-3|\mathbf{r}_i-\mathbf{r}_j|^2}{4S_s^2}\right), \quad (11)$$

where $\nu=\sigma_k^3$ is the excluded-volume interaction parameter, $N_{ks}=19.8$ is the number of Kuhn segments per spring, and $S_s^2=(N_{ks}/6)\sigma_k^2$ is the characteristic size of the coarse-grained beads.

An experimentally determined force-extension relation is used to calculate the elastic force on a bead [34]:

$$\mathbf{f}_{\mathbf{ij}}^{\mathbf{s}} = \frac{k_B T}{2\sigma_k}\left[\left(1 - \frac{|\mathbf{r_j} - \mathbf{r_i}|}{N_{ks}\sigma_k}\right)^2 + 4\frac{|\mathbf{r_j} - \mathbf{r_i}|}{N_{ks}\sigma_k} - 1\right]\frac{\mathbf{r_j} - \mathbf{r_i}}{|\mathbf{r_j} - \mathbf{r_i}|}. \quad (12)$$

This was found when measuring the force-extension relation for the entire chain. The force-extension relation is accurate when $N_{ks} \gg 1$, and we apply this equation to single chain segments of $N_{ks}=19.8$.

The fluid exerts a frictional force on the beads, given by

$$\mathbf{F}_f = -\zeta(\mathbf{u}_p - \mathbf{u}_f), \quad (13)$$

where $\mathbf{u}_p$ is the velocity of the bead, $\mathbf{u}_f$ is the velocity of the fluid at the bead position, $\zeta = 6\pi\eta a$ is the friction coefficient, and a is the hydrodynamic radius of the bead [23]. The simulation lattice size Δx is chosen to be 0.5 μm. For our model DNA chain, each bead has a hydrodynamic radius of $a = 0.077$ μm, or $0.154\Delta x$ [32,35]. Since the beads' positions are not limited to the lattice where the fluid velocity is well defined, $\mathbf{u}_f$ at the position of the bead is determined by linearly interpolating the velocities of the nearest-neighbor lattice sites such that $\mathbf{u}_f = \Sigma_{i \in NN} w_i \mathbf{u}_i$. The weighting factors w_i are normalized and $\mathbf{u}_i$ represents the fluid velocity at site i. The momentum transfer to the bead is $\Delta\mathbf{j} = -\mathbf{F}_f \Delta t / \Delta x^3$. The bead will also transfer this momentum to the fluid. The momentum transfer from the bead to a neighbor site i with velocity q is $\Delta\mathbf{f}_i = w_i \rho a_{c_q} \Delta\mathbf{j} \cdot \mathbf{c}_q$ [23].

The beads also undergo Brownian motion. The thermal fluctuations of the beads will be drawn from a Gaussian distribution with zero mean and a variance that varies with the bead height: $\sigma_v = 2k_B T(y)\zeta\Delta t$. Here,

$$T(y) = \frac{2(T_{hot} - T_{cold})}{Y_{max}}|(Y_{max}/2 - y)| + T_{cold}, \quad (14)$$

where Y_{max} is the width of the channel, y is the position of the bead in the channel, T_{hot} is the maximum, and T_{cold} is the minimum temperature in the channel. This leads to a sawtooth shape of the temperature plotted as a function of y. It should be noted that the temperature gradient in the system is only implemented here; all other forces and fluid properties are independent of location.

For this work, 50 polymers were simulated in a container of size 20 μm $\times$ 20 μm $\times$ 20 μm. Periodic boundary conditions were imposed in all directions unless otherwise noted. The time step for the fluid is $\Delta\tau = 8.8 \times 10^{-5}$ s and for the polymer $\Delta t = 1.72 \times 10^{-5}$ s as calculated using $T = T_{cold}$. The total simulation time was 1760 s. Data were recorded once every 17.6 s; the final 40 time steps were used to determine D_T.

III. RESULTS

A. Thermal migration of DNA

As shown in Fig. 1, the DNA accumulates in the center of the channel where the temperature minimum is found. The simulations with a larger temperature gradient result in a larger concentration gradient. The profile is nearly flat when the temperature is uniform in the channel. These results are in qualitative agreement with the work of Duhr, Arduini, and Braun [5].

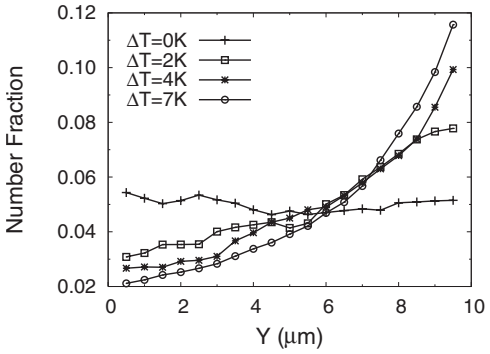

FIG. 1. Number fraction n/n_{total} where n is the number of beads whose center of mass is between $y-0.25$ and $y+0.25$ and n_{total} is the total number of beads, as a function of height for λ-DNA subjected to different temperature gradients. Data are averaged over the final 40 time steps of five simulations started from different random initial conditions. Shown is the average of the two mirror-image halves of the periodic system.

For quantitative comparison, we use the same equation found in [5]:

$$\frac{c(z)}{c_0} = \exp[-S_T(T(z) - T_0)], \quad (15)$$

where $c(z)$ is the concentration of DNA at position z, c_0 is the maximum concentration, $T(z)$ is the temperature at z, T_0 is the temperature at the position of c_0, and S_T is the Soret coefficient. This equation is derived from Eq. (1) with $J_y = 0$ and $c \ll 1$. The average Soret coefficient was found by fitting the density profile to Eq. (15) and solving for S_T. As in [5], we use $D = 1.0$ μm^2/s for λ-DNA to calculate D_T from S_T.[1] We find, for the data presented in Fig. 1, $D_T = 0.38 \pm 0.1$ μm^2/s K. This is in good agreement with the value of 0.4 μm^2/s K reported in [5].

In the experiments reported in [5,9,10], nearly identical thermal diffusion coefficients were measured for different molecular weights of DNA and other polymers. We find similar values of D_T for

$$19.4 \text{ kbp } [D_T = 0.46 \pm 0.06 \ \mu\text{m}^2/\text{s K}],$$

$$48.5 \text{ kbp } [D_T = 0.40 \pm 0.06 \ \mu\text{m}^2/\text{s K}],$$

and

$$67.9 \text{ kbp DNA } [D_T = 0.40 \pm 0.06 \ \mu\text{m}^2/\text{s K}]$$

for $\Delta T = 4$ K. The diffusion coefficient D of the individual molecules was calculated according to

[1] To compare with the experimental results quantitatively, we use the same value for the molecular diffusion coefficient of λ-DNA. However, an experimentally determined value of $D = 0.48$ μm^2/s was reported by Smith, Perkins, and Chu [41]. Using this value would decrease D_T by a factor of 0.48.

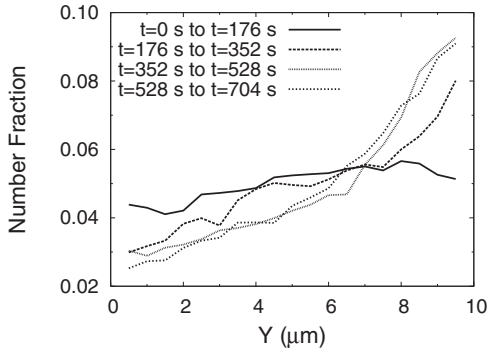

FIG. 2. Number fraction n/n_{total} where n is the number of beads whose center of mass is between $y-0.25$ and $y+0.25$ and n_{total} is the total number of beads, as a function of height at different times for λ-DNA with $\Delta T=4$ K. Data are averaged over ten time steps of five simulations started from different random initial conditions. Shown is the average of the two mirror-image halves of the periodic system.

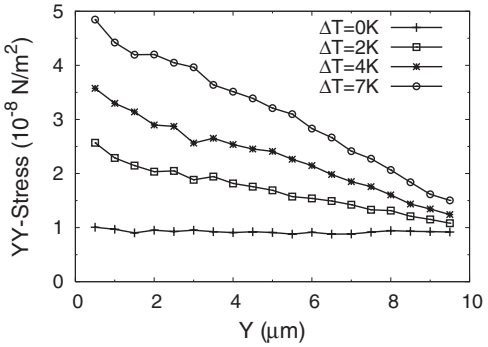

FIG. 3. Stress in the y direction across the channel for λ-DNA. Data are averaged over the final 40 time steps of five simulations started from different random initial conditions. Shown is the average of the two mirror-image halves of the periodic system.

$$D_L = D_\lambda \left(\frac{L}{L_\lambda} \right)^{-0.588}, \tag{16}$$

where D_λ is 1 $\mu m^2/s$ (see footnote 1), L is the length of the DNA, L_λ is 48.5 kbp, the length of λ-DNA, and D_L is the molecular diffusion coefficient for DNA of length L[32].

The development of the density profile over time can be seen in Fig. 2. The profile develops slowly, and only after more than 300 s does the system reach steady state. This time frame is similar to that observed by Duhr, Arduini, and Braun who report that several hundred seconds are needed to reach the steady state [5].

B. Mechanism of thermal migration

To understand why the polymers migrate to the colder regions, we investigated the dynamics of the solvent. Since the properties of the fluid were kept constant across the channel, the migration must result from interactions between the fluid and the polymers. Thus the momentum flux of the fluid within two lattice sites of a bead was recorded. This quantity is known to be coupled to the DNA fluctuations [23] and will contribute to the local fluid stress [36]. A gradient in $\Pi_{yy} = \Sigma_i n_i^{eq} \cdot \mathbf{c}_i \mathbf{c}_i$ is observed for nonzero-temperature gradient but is absent for simulations with uniform temperature as seen in Fig. 3. As gravity is absent, the stress is only due to the momentum flux [36]. This gradient in flux is therefore a gradient in stress which causes the polymers to migrate into the cold regions.

The difference in stress is due solely to the interaction of the beads and the fluid. Without the presence of the DNA, the fluid will relax back to equilibrium conditions and therefore uniform stress across the channel. In fact, when the force the polymers exert on the fluid is set to zero in the simulation, no thermal diffusion is observed. Thus the fluctuations of the polymers induce a local, short-lived gradient in stress which causes the thermal migration of the species.

The steady state is reached when the particle flux from the cold region to the hot region equals the flux in the reverse direction. The particles will migrate only because of Brownian motion in this simulation. Thus there is a well-defined probability of a particle in the cold side receiving a sufficient Brownian kick to move to a higher-stress region. In the steady state, this probability times the number of beads in the cold side must equal the corresponding probability a particle will move towards the low-stress area times the number of beads in the hot region. Since the Brownian force depends on the viscosity of the fluid and the hydrodynamic radius of the particle, the thermal diffusion coefficient should also depend on these parameters. We will investigate these dependences within the limits of our simulation.

C. Particle size effects

The polymer and fluid are coupled through the Brownian and viscous forces. Both terms depend on $\zeta = 6\pi\eta a$—the viscous force explicitly and the Brownian term through the standard deviation of the distribution of the fluctuations. In the simulation, neither the hydrodynamic radius a nor viscosity of the fluid, η, appears singly. Thus, doubling the value of one term is analogous to doubling the other. However, we consider changes to ζ to be changes to a since experimental work has been conducted on the effects of changing the colloidal particle diameter rather than changing the viscosity of the fluid [12,13].

The simulations were conducted using 100 individual spheres not attached to each other by springs. We investigated particles with a hydrodynamic radius of 0.0385, 0.077, 0.154, and 0.231 μm with a temperature difference of 4 K across the 10-μm channel. The diffusion coefficient D of each species was calculated according to $D = k_B T_{cold}/6\pi\eta a$ where a is the hydrodynamic radius of the particle and η is the viscosity of the solution. Similar values were obtained for the Soret coefficient S_T as can be seen in Fig. 4. Here, the density profiles are nearly identical for all diameters. However, because of the different diffusion coefficients D, larger values for D_T were obtained for the smaller particles. See Table I for a comparison of values. It has been suggested that D_T decreases with increasing a because the gradient is too steep to allow the particles to reach local equilibrium. We therefore decreased the temperature difference to 2 K to test

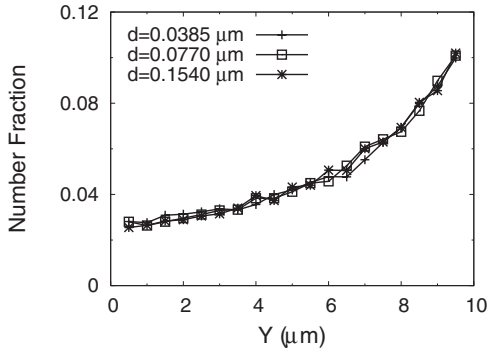

FIG. 4. Number fraction n/n_{total} where n is the number of beads whose center of mass is between $y-0.25$ and $y+0.25$ and n_{total} is the total number of beads, as a function of height for spherical particles of different diameter with $\Delta T=4$ K. Data are averaged over the final 40 time steps of five simulations started from different random initial conditions. Shown is the average of the two mirror-image halves of the periodic system.

this hypothesis. However, as Table I shows, the values of D_T do not change appreciably. This suggests the decrease of D_T with increasing radius is not due to particles being farther out of local equilibrium. Indeed, all of the above simulations meet the criterion $(aS_T)^{-1} > \nabla T$, as set by the local equilibrium condition in [13].

We suggest a different explanation based on the analysis of the nonequilibrium stress induced by the thermal gradient. The fluid stress gradient can be seen in Fig. 5. The larger-diameter particles induce a steeper gradient in the stress than do the smaller spheres. However, the steady-state density profile is the same for all particles due to the differences in the Brownian force on the particles. Since the standard deviation of the distribution is proportional to the hydrodynamic radius, larger particles experience larger fluctuations. This is exactly balanced by the steeper gradient induced, leading to steady-state density profiles that are nearly the same for all particle sizes.

IV. CONCLUSIONS

We use a lattice-Boltzmann simulation to investigate the mechanism behind thermal diffusion of λ-DNA and spherical particles. This method allows us to capture the nonequilibrium stress in the fluid due to the temperature gradient. We find good agreement with experimental results for the thermal diffusion coefficient D_T for λ-DNA [5]. It is also observed that D_T decreases as the diameter a of diffusing spherical particles increases in partial agreement with experiments by Shiundu *et al.* [12]. Recent experiments by Duhr and Brann have shown different qualitative dependence as predicted by our simulations [11]. However, this may be attributed to the presence of long-range electrostatic interactions in the experiments. Our simulations have treated the DNA as an uncharged polymer, corresponding to experiments in which the electrostatic interactions are highly screened. Future work will investigate the role of electrostatic interactions and the role of counterions on the thermodiffusion of DNA molecules.

TABLE I. Values of the thermal diffusion coefficient D_T given in $\mu m^2/s\,K$ for spheres of different hydrodynamic radius a and temperature difference ΔT across the 10-μm channel.

ΔT	$a=0.0385$ μm	$a=0.077$ μm	$a=0.154$ μm
4 K	2.1±0.3	1.12±0.06	0.59±0.04
2 K	2.3±0.4	1.1±0.2	0.60±0.01

The thermal diffusion coefficient is observed to decrease if the size of the diffusing species is increased. In our work, unlike in experiments, the fluid characteristics such as viscosity are held constant across the channel. It is also noted that decreasing the temperature difference across the channel did not change these results. Therefore the dependence on particle size cannot be explained as a result of the spheres not reaching local equilibrium with the fluid or the fluid characteristics varying too much across the channel.

Instead, the nonequilibrium component of the fluid flow is observed to be linked with the migration of the solute. The induced stress is significantly more in the hot region than in the cold. Thus particles will migrate to the cold regions. The thermal diffusion coefficient will therefore depend on factors influencing the interaction between the solvent and solute.

This picture is in agreement with the theoretical work of several authors [8,16–21] who investigate local pressure gradients induced by nonisotropic interactions between the solute and solvent. However, in those studies, the specifics of the interaction of the diffusing particle and surrounding fluid played an important role in determining S_T. Here, we have quantitatively predicted the thermal diffusion coefficient of DNA as well as the time scales of the phenomenon without including the details of the interaction between the polymer and solvent. Instead of these characteristics being important, only the Brownian motion of the particle induces a local stress gradient in the fluid. This may indicate that hydrodynamic memory effects, already shown to be important in the

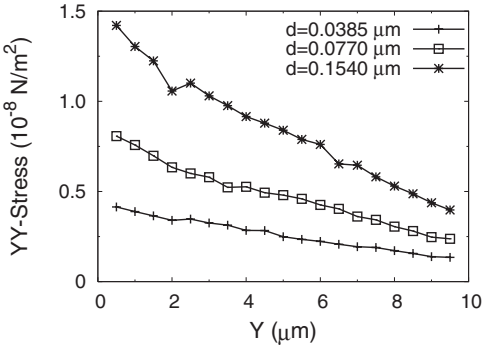

FIG. 5. Stress in the y direction across the channel for spherical particles of different diameter. Data are averaged over the final 40 time steps of five simulations started from different random initial conditions. Shown is the average of the two mirror-image halves of the periodic system.

mass diffusion of polymers and colloids, should be considered when developing theories of thermal diffusion [37–40]. We therefore hope that this work will inspire new directions in theoretical examinations of thermal diffusion.

ACKNOWLEDGMENTS

This work was supported by a grant from the Li Foundation and Grant No. NSC 95-2112-M-001-051-MY3 from the National Science Council of Taiwan.

[1] C. Ludwig, Sitzungsber Akad. Wiss. Wien Math.-Nat. Wiss. Kl. **20**, 539 (1856).
[2] C. Soret, Arch. Sci. Phys. Nat. **2**, 48 (1879).
[3] S. Wiegand, J. Phys.: Condens. Matter **16**, R357 (2004).
[4] R. Khare, M. D. Graham, and J. J. de Pablo, Phys. Rev. Lett. **96**, 224505 (2006).
[5] S. Duhr, S. Arduini, and D. Braun, Eur. Phys. J. E **15**, 277 (2004).
[6] S. Iacopini and R. Piaza, Europhys. Lett. **63**, 247 (2003).
[7] R. Kita, S. Wiegand, and J. Luettmer-Strathmann, J. Chem. Phys. **121**, 3874 (2004).
[8] R. Piazza and A. Guarino, Phys. Rev. Lett. **88**, 208302 (2002).
[9] W. Köhler, C. Rosenauer, and P. Rossmanith, Int. J. Thermophys. **16**, 11 (1995).
[10] K. Zhang, M. Briggs, R. Gammon, and J. Sengers, J. Chem. Phys. **111**, 2270 (1999).
[11] S. Duhr and D. Braun, Proc. Natl. Acad. Sci. U.S.A. **103**, 19678 (2006).
[12] P. Shiundu, P. Williams, and J. Giddings, J. Colloid Interface Sci. **266**, 366 (2003).
[13] S. Duhr and D. Braun, Phys. Rev. Lett. **96**, 168301 (2006).
[14] H. Brenner, Phys. Rev. E **74**, 036306 (2006).
[15] H. Brenner, Physica A **349**, 10 (2005).
[16] E. Ruckenstein, J. Colloid Interface Sci. **83**, 77 (1981).
[17] S. N. Semenov and M. Schimpf, Phys. Rev. E **69**, 011201 (2004).
[18] A. Parola and R. Piazza, Eur. Phys. J. E **15**, 255 (2004).
[19] K. I. Morozov, Phys. Rev. E **53**, 3841 (1996).
[20] K. Morozov, in *Thermal Nonequilibrium Phenomena in Fluid Mixtures*, edited by S. Wiegand and W. Köhler (Springer, Berlin, 1999), p. 38.
[21] J. Bafaluy, I. Pagonbarraga, J. Rubí, and D. Bedeaus, Physica A **213**, 277 (1995).
[22] E. Bringuier and A. Bourdon, Phys. Rev. E **67**, 011404 (2003).
[23] P. Ahlrichs and B. Dünweg, Int. J. Mod. Phys. C **9**, 1429 (1998).
[24] P. Ahlrichs and B. Dünweg, J. Chem. Phys. **111**, 8225 (1999).
[25] O. Berk Usta, A. Ladd, and J. Butler, J. Chem. Phys. **122**, 094902 (2005).
[26] O. Berk Usta, J. Butler, and A. Ladd, Phys. Fluids **18**, 031703 (2006).
[27] A. Ladd and R. Verberg, J. Stat. Phys. **104**, 1191 (2001).
[28] A. Ladd, J. Fluid Mech. **271**, 285 (1994).
[29] R. Benzi, S. Succi, and M. Vergassola, Phys. Rep. **222**, 145 (1992).
[30] P. Bhatnagar, E. Gross, and M. Krook, Phys. Rev. **94**, 511 (1954).
[31] R. M. Jendrejack, E. T. Dimalanta, D. C. Schwartz, M. D. Graham, and J. J. de Pablo, Phys. Rev. Lett. **91**, 038102 (2003).
[32] R. Jendrejack, D. Schwartz, M. D. Graham, and J. J. de Pablo, J. Chem. Phys. **119**, 1165 (2003).
[33] R. Jendrejack, E. Dimalanta, D. Schwartz, M. D. Graham, and J. J. de Pablo, J. Chem. Phys. **116**, 7752 (2002).
[34] C. Bustamante, Z. Bryant, and S. Smith, Nature (London) **421**, 423 (2003).
[35] Y. L. Chen, H. Ma, M. D. Graham, and J. J. dePablo, Macromolecules (to be published).
[36] S. Chapman and T. Cowling, *The Mathematical Theory of Non-uniform Gases* (Cambridge University Press, Cambridge, England, 1991).
[37] E. Hinch, J. Fluid Mech. **72**, 499 (1975).
[38] G. Nägele and P. Baur, Europhys. Lett. **38**, 557 (1997).
[39] V. Lisy, J. Tothova, B. Brutovsky, and A. Zatovsky, in *Soft Condensed Matter: New Research*, edited by K. Dillon (Nova Science, New York, 2005).
[40] B. Lukić, S. Jeney, C. Tischer, A. J. Kulik, L. Forró, and E.-L. Florin, Phys. Rev. Lett. **95**, 160601 (2005).
[41] D. E. Smith, T. T. Perkins, and S. Chu, Macromolecules **29**, 1372 (1996).